Strotos, G., Koukouvinis, P., Theodorakakos, A., Gavaises, M. & Bergeles, G. (2015). Transient heating effects in high pressure Diesel injector nozzles. International Journal of Heat and Fluid Flow, 51, pp. 257-267. doi: 10.1016/j.ijheatfluidflow.2014.10.010

Transient heating effects in high pressure Diesel injector nozzles

George Strotos[1,a,*], Phoevos Koukouvinis[1,b], Andreas Theodorakakos[1,c],ManolisGavaises[1,d]and George Bergeles[1,e]

[1]School of Engineering and Mathematical Sciences, City University London, Northampton Square, EC1V 0HB, London, UK

[a] George.Strotos.1@city.ac.uk

[b] Foivos.Koukouvinis.1@city.ac.uk

[c] Andreas.Theodorakakos.1@city.ac.uk

[d] M.Gavaises@city.ac.uk

[e] bergeles@fluid.mech.ntua.gr

[*]Corresponding author

Abstract

The tendency of today's fuel injection systems to reach injection pressures up to 3000 bar in order to meet forthcoming emission regulations may significantly increase liquid temperatures due to friction heating; this paper identifies numerically the importance of fuel pressurization, phase-change due to cavitation, wall heat transfer and needle valve motion on the fluid heating induced in high pressure Diesel fuel injectors. These parameters affect the nozzle discharge coefficient (C_d), fuel exit temperature, cavitation volume fraction and temperature distribution within the nozzle. Variable fuel properties, being a function of the local pressure and temperature are found necessary in order to simulate accurately the effects of depressurization and heating induced by friction forces. Comparison of CFD predictions against a 0-D thermodynamic model, indicates that although the mean exit temperature increase relative to the initial fuel temperature is proportional to ($1-C_d^2$) at fixed needle positions, it can significantly deviate from this value when the motion of the needle valve, controlling the opening and closing of the injection process, is taken into consideration.Increasing the inlet pressure from 2000bar, which is the pressure utilized in today's fuel systems to 3000bar, results to significantly increased fluid temperatures above

the boiling point of the Diesel fuel components and therefore regions of potential heterogeneous fuel boiling are identified.

Keywords: nozzle, cavitation, variable properties, moving needle, fuel heating

1 Introduction

The market share for passenger cars is expected to double (ExxonMobil) the coming years, as also the diesel oil consumption. The need for more efficient IC engines which comply with the strict emission legislation to be imposed leads to the development of higher injection pressures, pressures up to 3000bar(Goud M et al., 2012) from 2000 bar, which is the nominal value in today's commercial passenger car fuel injection equipment (FIE). At such elevated pressures high flow velocities develop within the injector which lead to cavitation (Arcoumanis et al., 2000). Cavitation in fuel injectors has been examined both experimentally and numerically as it reduces injection volumetric efficiency and may result to material erosion(Prosperetti and Hao, 1999). On the other hand, it may improve the air-fuel mixing by increasing the spray cone angle(Payri et al., 2004). Flow measurements in cavitating injector nozzles operating under such pressures have not been obtained so far; most of the experimental studies reported are emulating the engine operating conditions as in (Andriotis et al., 2008; Badock et al., 1999; Blessing et al., 2003; Chaves et al., 1995; Payri et al., 2013; Soteriou et al., 2000). Alternatively, computational methodologies seem to be the only way to understand the implications of cavitation under real operating conditions. Several numerical methodologies for simulating cavitation have been proposed. For example, a single-fluid mixture is proposed in(Chen and Heister, 1995) while the two-fluid method is reported in (Alajbegovic et al., 1999; Singhal et al., 2002; Yuan and Schnerr, 2004) where conservation equations are solved for both phases separately and interaction between them is accounted for by using additional source terms. The Eulerian-Lagrangian models of (Brennen, 1995; Giannadakis et al., 2004; Hilgenfeldt et al., 1998; Keller and Miksis, 1980) assume a bubbly phase to be dispersed inside the liquid phase while the Rayleigh-Plesset equation is utilized for predicting the bubble's growth and collapse. The models of(Ando et al., 2011; Fuster and Colonius, 2011; Jamaluddin et al., 2011;Zeravcic et al., 2011) account for compressibility effects. Homogeneous equilibrium models (HEM) assume a perfect mixing between the liquid and the vapor phase while the cavitation bubble's growth is calculated by using a barotropic equation which relates pressure and density (Habchi et al., 2008; Liu et al., 2004; Payri et al., 2012; Salvador et al., 2013).

A common feature of cavitation studies in fuel injector nozzles is the assumption of isothermal flow due to the short timescales involved. On the other hand, the flow induced during the discharge of the fuel is characterized by strong velocity gradients which induce wall friction and consequently fuel heating. Studies addressing the complicated effects occurring during the motion of the needle valve that controls the injection process have recently appeared in the literature (Battistoni and Grimaldi, 2012; He et al., 2013; Lee and Reitz, 2010; Margot et al., 2010; Neroorkar et al., 2012; Payri et al., 2009; Zhao et al., 2013). The present study focuses on the thermal effects occurring in high pressure diesel nozzles by solving the energy equation and including the friction induced heating. The CFD model used is an Eulerian-Lagrangian model which has been built upon the in-house CFD cavitation model reported in (Giannadakis et al., 2008); this work is an extension of that presented recently in (Strotos et al., 2014a; Strotos et al., 2014b; Theodorakakos et al., 2014) which additionally examines the effect of needle motion. In the absence of relevant experimental data, the present work aims to quantify the numerical effects of using constant or variable properties, the effect of two-phase flow, the effect of inlet pressure increase and the effect of initial and boundary conditions on temperature distribution within the injector. In the following sections, the mathematical model is presented, followed by the results obtained for high pressure diesel nozzles in steady lift and moving lift cases; the most important conclusions are summarized at the end.

2 Numerical model and methodology

2.1 Equations solved

The flow solver used has been developed by the authors' group and solves the Navier-Stokes equations in an unstructured mesh. Turbulence is modeled with the k-ε model (Launder and Spalding, 1974); detailed description of the flow equations can be found in (Giannadakis et al., 2008). Here, focus is given into the solution of the energy equation for the liquid phase and the determination of the temperature field. Based on (Städtke, 2007), the conservation equation expressed in terms of the specific total enthalpy is:

$$\frac{\partial(a_L \rho h_{tot})}{\partial t} + \nabla\cdot(a_L \rho h_{tot} \mathbf{u}) = \nabla\cdot(a_L \kappa_{eff} \nabla T) + \nabla\cdot(a_L \boldsymbol{\tau}_{eff}\cdot\mathbf{u}) + a_L \rho(\mathbf{u}\cdot\mathbf{g}) + \frac{\partial(a_L p)}{\partial t} + S_h \quad (1)$$

Where the specific total enthalpy is the sum of the specific static enthalpy h, the flow mean kinetic energy and the turbulent kinetic energy k

$$h_{tot} = h + \frac{\mathbf{u} \cdot \mathbf{u}}{2} + k \tag{2}$$

The presence of the cavitating phase is taken into account through α_L which represents the liquid volume fraction in a computational cell, and with the source term S_h (Städtke, 2007) which accounts for the interaction between the two phases, gas and liquid. This additional source term for the interaction between the two phases includes the energy exchange due to mass transfer, the interfacial heat transfer and the work of viscous interfacial forces. Note that equation (1) reduces to the equation given in (Versteeg and Malalasekera, 2007) for the case of single phase flow. In (1) the stress tensor $\boldsymbol{\tau}_{eff}$ is given by:

$$\boldsymbol{\tau}_{eff} = \mu_{eff} \left(\nabla \mathbf{u} + (\nabla \mathbf{u})^T \right) - \frac{2}{3} \mu_{eff} (\nabla \cdot \mathbf{u}) \mathbf{I} - \frac{2}{3} \rho k \mathbf{I} \tag{3}$$

$$\mu_{eff} = \mu_{lam} + \mu_{turb} \tag{4}$$

$$\kappa_{eff} = \left(\frac{\mu_{lam}}{Pr_{lam}} + \frac{\mu_{turb}}{Pr_{tutb}} \right) c_p \tag{5}$$

Where $\mathbf{I}$ is the unit tensor. The turbulent viscosity μ_{turb} is calculated from the k-ε turbulence model and the turbulent Prandtl number Pr_{turb}, is taken equal to 0.85. It has to be noted that the 2nd RHS term of equation (1) contains both the reversible and the irreversible work of viscous forces; the latter is commonly known as viscous heating and represents the heating induced by the friction forces.

Following the methodology presented in (Kolev, 2002), the specific enthalpy can be expressed as

$$h = h_0 + c_{pmT} (T - T_0) + h^* \tag{6}$$

$$c_{pmT} = \left(\int_{T_0}^{T} c_p dT \right) / (T - T_0) \tag{7}$$

$$h^* = \int_{p_0}^{p} \left(\frac{\partial h}{\partial p} \right)_{T = T_0} dp \tag{8}$$

In these equations h_0, p_0, and T_0, are reference values, h^* is a function of pressure, while c_{pmT} is the mean heat capacity between the temperature under consideration and a reference temperature T_0. For the case of constant properties, c_{pmT} is simply equal to c_p, while $h^*=(p-p_0)/\rho$. The reason for adopting the methodology of (Kolev, 2002) is that the author gives these thermodynamic properties as a function of pressure and temperature in the range 0-2500bar and 0-120°C.

For reasons of numerical stability, the diffusion term appearing on the RHS of equation (1) and containing the temperature instead of the total enthalpy is treated in an implicit way. Solving equation (6) for T and substituting it in (1)after some manipulation the following transport equation for the specific total enthalpy is derived:

$$\begin{aligned}\frac{\partial\left(a_L\rho h_{tot}\right)}{\partial t}+\nabla\cdot\left(a_L\rho h_{tot}\mathbf{u}\right)=\nabla\cdot\left(a_L\Gamma\nabla h_{tot}\right)+\nabla\cdot\left(a_L\boldsymbol{\tau}_{eff}\cdot\mathbf{u}\right)+a_L\rho\left(\mathbf{u}\cdot\mathbf{g}\right)+\frac{\partial\left(a_L p\right)}{\partial t}+S_h\\ -\nabla\cdot\left(a_L\Gamma h_{tot}\frac{\nabla c_{pmT}}{c_{pmT}}+a_L\Gamma c_{pmT}\nabla\left(\frac{h_{add}}{c_{pmT}}\right)\right)\end{aligned} \tag{9}$$

$$\Gamma=\frac{\mu_{lam}}{Pr_{lam}}+\frac{\mu_{turb}}{Pr_{tutb}} \tag{10}$$

$$h_{add}=h^*+\frac{\mathbf{u}\cdot\mathbf{u}}{2}+k \tag{11}$$

In each iteration the total enthalpy equation is solved and the temperature is obtained either from equation (6) for the case of constant properties, or from an iterative procedure in the case of variable properties. When the temperature has been determined, the properties are updated from the known temperature and pressure field. This procedure requires no more than 10 internal iterations to converge while an under-relaxation factor can be also used in updating the temperature.

Regarding the impact of source term S_h in equation (9), an order of magnitude analysis has revealed that its impact in fuel heating, could be ignored. The rate of vapor formation is more than 5 orders of magnitude smaller than the fuel flow rate, while the heat flux due to vaporization is even smaller compared to the energy of the fuel entering the injector. Thus the main parameter affecting the fuel heating is the friction forces due to the strong velocity gradients appearing in the near wall region.

2.2 Fuel properties

The fuel used is the so-called "summer diesel" and its properties were taken from (Kolev, 2002) as function of temperature and pressure. For the purposes of the present work, they have been extrapolated up to 3000bar and 400°C for all cases simulated. The extrapolation method adopted, uses the functions given in (Kolev, 2002) but extents the limits of pressure and temperature up to the point at which the property under consideration reaches a local minimum or maximum; beyond this point, each property is assumed to be equal to the corresponding value of the local minimum or maximum. The fuel properties utilized are shown in Fig.1.

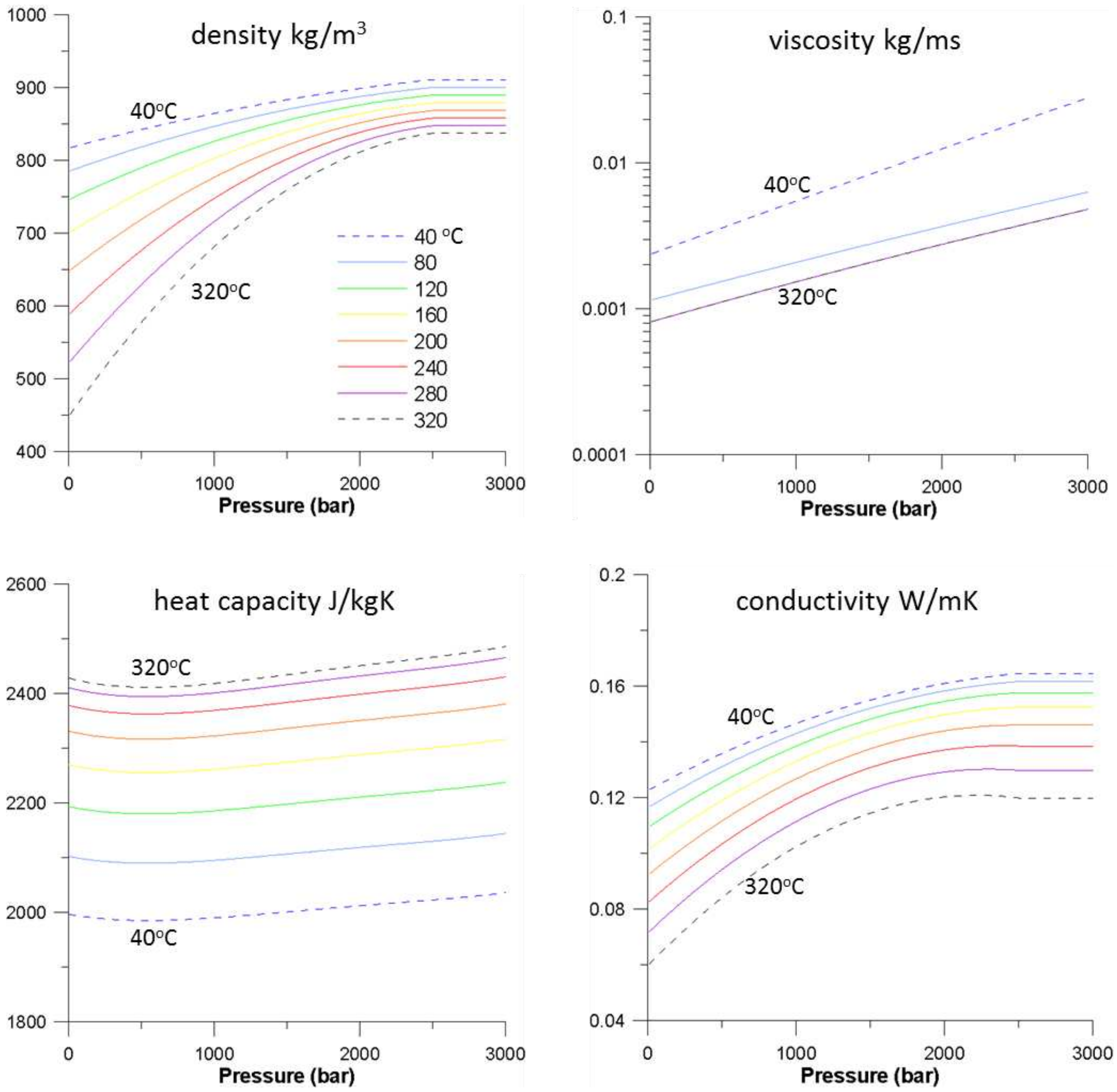

Fig.1: Diesel fuel properties as a function of pressure for selected temperature values (extrapolated from 2400 to 3000bar and 120 to 400°C).

2.3 Implementation of needle motion

The computational technique used to simulate the needle motion is summarized in Fig.2. It can be divided into two stages. In the first stage, three grids (termed as “initial grids”) are constructed at 10, 60 and 150μm needle lifts. Stretching of the three “initial grids” to both lower and higher needle lifts is performed resulting to three pairs of “base grids”; for the particular nozzle simulated here, the three pairs of ‘base grids’ have been obtained atthe following lifts: 5 and 35μm, 25 and 120μm, and 110 and 230μm, respectively. This procedure is graphically represented in Fig.2a. Note that each pair of the “basic grids” have identical number of cells and identical grid topology at the boundary faces of the needle and the nozzle wall. It has also to be noted that overlapping regions exist between 25 and 35μm and between 110 and 120μm.

During the needle motion (Fig.2b), the grid for each needle lift is obtained by linear interpolation between a pair of “base grids”. When the needle lift value falls within an overlapping region, then the obtained solution is remapped to the other pair. Special care has been taken in order to construct grids with similar topology and minimize computational errors when the grid is remapped. With regards to temporal discretization, a fully implicit scheme was used, which is unconditionally stable, while shorter computational time steps have been used in the opening and closing phase of the needle valve in order to ensure that the needle lift does not change more than 1.0μm/time-step; this limitation was used to avoid abrupt changes in the grid topology. Numerical experiments have indicated that the opening phase is not affected by the chosen time-step. On the other hand, during the closing phase, some differences exist especially at the last stages, in which compressibility effects may however become important but the code used does not account for such phenomena.

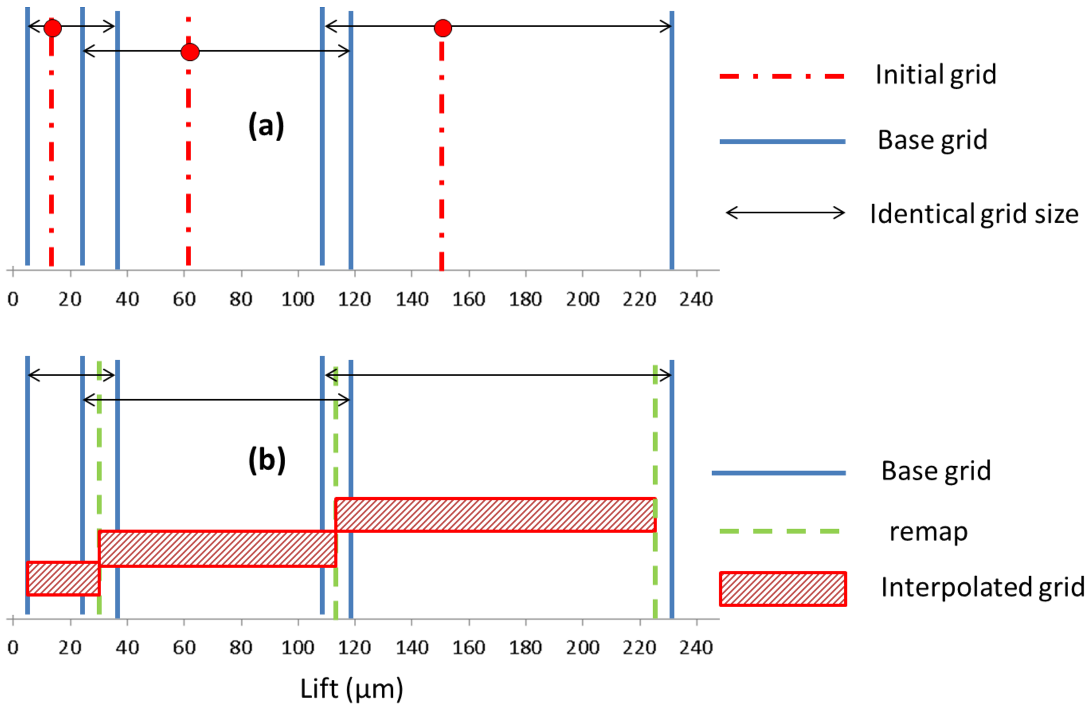

Fig.2: Computational technique for the grid adaption in moving lift.

3 Results and discussion

3.1 Cases examined

A 6-hole tapered nozzle with 0.175mm hole diameter has been used in the present investigation; a similar geometry was used in the past for numerically validating an iso-thermal cavitation model (Giannadakis et al., 2007). The tapered hole has 20μm rounding at the inlet of the hole and the k-factor is 1.77 (defined as (D_{in} - D_{out})/10μm). For the purposes of the present simulation, the 1/6th sector of the nozzle was modeled by applying symmetry boundary conditions at the cross sections; numerical experiments using grid sizes from 0.38M cells up to 3.4M cells prove that a grid of approximately one million cells was adequate for grid independent results to be achieved. The maximum variation of discharge coefficient was approximately 0.02 (i.e. 4%), while the maximum variation for the mean temperature increase was 1.6°C for the various lifts examined. The maximum temperature variations between different grids observed locally at the exit of the hole may reach up to 5°C which are considered to be small compared to the overall heating of the fuel. Furthermore, 10-25 cell layers were used inside the gap between the needle seat and the body of the nozzle, which ensures the capturing of the velocity and thermal boundary layer development. Details of the nozzle geometry and grid details are presented in Fig.3.

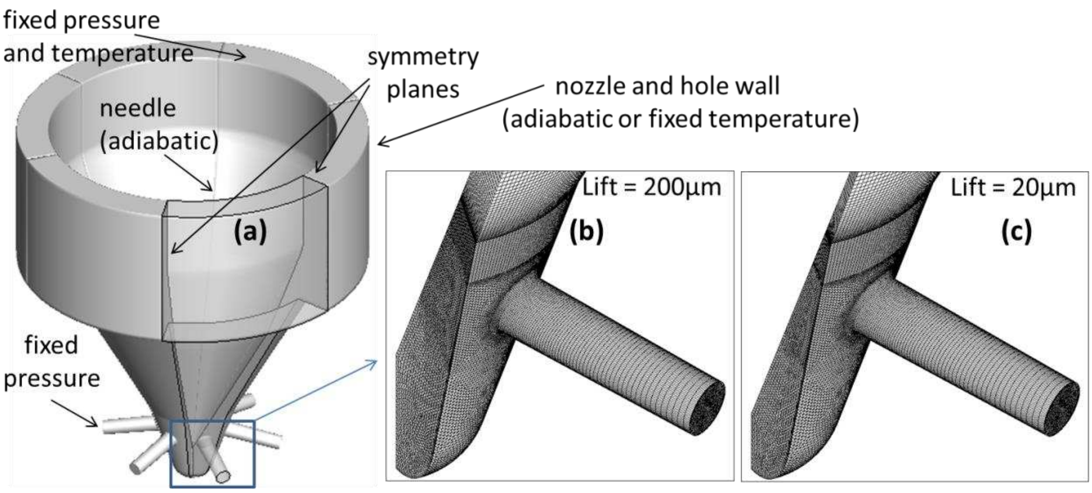

Fig.3: Nozzle geometry and grid details. (a)Computational domain and boundary conditions utilized, (b, c) Detail of the computational mesh at 200μm and 20μm needle lift respectively.

The test cases simulated and the boundary conditions used are listed in Table 1and Table 2, respectively, covering a wide range of fixed needle lift positions (varying from 5 up to 200μm) and transient simulations with a moving lift, while in both cases (fixed or moving lift) the differences between single and two-phase flow are examined. Additionally, the effect of using constant or variable fuel properties is quantified. Two inlet pressures are examined (2000 and 3000bar) with fixed inlet temperature at 80°C; at the nozzle hole exit a fixed pressure equal to 60bar has been utilized. The needle's wall was assumed to be adiabatic, while for the nozzle's wall either adiabatic or constant temperature at 80°C and 300°C boundary conditions were applied, since its temperature is not generally known. The flow field in the near wall region was modelled by using wall functions along with the enhanced wall treatment proposed by (Wolfshtein, 1969); the y+ values in the wall region were varied between 1 and 30. Regarding the initial conditions for the transient cases, simulations start from a converged velocity field at 5μm lift, while the initial temperature field for the fuel was assumed to be uniform and equal to the inlet temperature for most of the cases examined. The effect of the initial liquid temperature distribution is further examined by considering the last case of Table 1 in which the liquid at the upper part of the injector has 80°C, the liquid at the lower part (including the region of the hole) has a temperature of 120°C and between them there is a region in which the liquid temperature varies linearly between 80°C and 120°C.

Table 1: Simulation cases

Lift [µm]	Inlet pressure (bar)	phases	properties	Nozzle wall	Initial condition for fuel temperature
5, 20, 40, 80, 200	2000, 3000	single	Constant	Adiabatic	Uniform (80ºC)
5, 20, 40, 80, 200	2000, 3000	single	Variable	Adiabatic	Uniform (80ºC)
20, 40, 80, 200	2000, 3000	two	Variable	Adiabatic	Uniform (80ºC)
Moving lift	2000, 3000	single	Variable	Adiabatic	Uniform (80ºC)
Moving lift	2000, 3000	two	Variable	Adiabatic	Uniform (80ºC)
Moving lift	2000	single	Variable	Fixed temperature(80/300ºC)	Uniform (80ºC)
Moving lift	2000	single	Variable	adiabatic	Linear (80-120ºC)

Table 2: Summary of boundary conditions.

magnitude	Inlet	exit	Needle wall	Nozzle wall
Static pressure	Fixed (2000, 3000bar)	Fixed (60bar)		
Velocity vector	Zero 1st gradient	Zero 1st gradient	No slip	No slip

temperature	Fixed (80°C)	Zero 1st gradient	adiabatic	Adiabatic or fixed (80/300°C)

3.2 Steady lift simulations

Due to lack of experimental data for the fuel heating in such high pressure Diesel injectors, a 0-D thermodynamic model is used to estimate the mean fuel heating and validate the present methodology. The model combines the continuity equation, the Bernoulli equation and the 1st law of thermodynamics. Assuming adiabatic nozzle walls and no work exchange in steady lift conditions, the pressure difference between inlet and exit (Δp) is converted to liquid kinetic energy and liquid heating for a given nozzle discharge coefficient. It has to be noted that the 0-D model ignores the contribution of turbulence (which is expected to have a minor effect), as also it is valid only for the case of single phase flow. For the case of constant properties fluid, it is easy to prove that the fuel increased temperature due to friction heating equals to:

$$\Delta T = \left(1 - C_d^2\right)\Delta T_{ref} \tag{12}$$

where

$$\Delta T_{ref} = \frac{\Delta p}{\rho_{in} c_{p,in}} \tag{13}$$

$$U_{ref} = \sqrt{\frac{2\Delta p}{\rho_{in}\left(1 - \left(A_{out}/A_{in}\right)^2\right)}} \tag{14}$$

$$C_d = \frac{\dot{m}}{\rho_{in} A_{out} U_{ref}} \tag{15}$$

The reference temperature difference ΔT_{ref} can serve as a non-dimensional parameter to compare different cases, thus enabling a direct comparison between cases involving constant or variable thermodynamic properties. The same comments apply also to the definition of reference velocity U_{ref} and discharge coefficient C_d which are calculated based on the inlet properties which are fixed.

In Fig.4 the fuel heating for the cases of 2000bar (a) and 3000bar (b) inlet pressure is presented. The dashed and the solid lines correspond to the 0-D model for constant and variable properties, respectively. As seen, the assumption of constant properties leads to overprediction of the fuel heating, while it is important to notice that the variable properties case leads to fuel sub-cooling for high C_d values. In this case the friction is low and the sub-cooling due to fuel depressurisation dominates the phenomenon. The difference between the two curves seems to be rather significant, which implies that variable properties are important for accurate estimation of the fuel heating. Comparing Fig.4a to Fig.4b it is concluded that the dimensionless fuel heating is quite similar for different inlet pressures; in dimensional quantities, the reference temperature difference ΔT_{ref} increases with inlet pressure which means that more fuel heating is expected for high inlet pressures. For all cases, CFD predictions are in good agreement with the 0-D model. These predictions were obtained by changing the needle lift (in the range 5-200μm) which in turn results in different values of the discharge coefficient. It is also important to notice that at the same valve lift, different discharge coefficient is predicted for constant and variable properties. At low lifts, the constant properties assumption leads to under-estimation of the discharge coefficient, while at high lift the constant properties assumption leads to discharge coefficient overestimation. The effect of two-phase flow is also presented in Fig.4 for the variable properties simulations. As seen, the discharge coefficient reduces relative to the single phase case due to the partial blockage of the flow from the bubbles, and also the fuel heating is slightly lower, since the friction forces are multiplied by the liquid volume fraction. The reduction of friction in cavitating flows has been also reported in (Payri et al., 2012) and (Javier López et al., 2012).

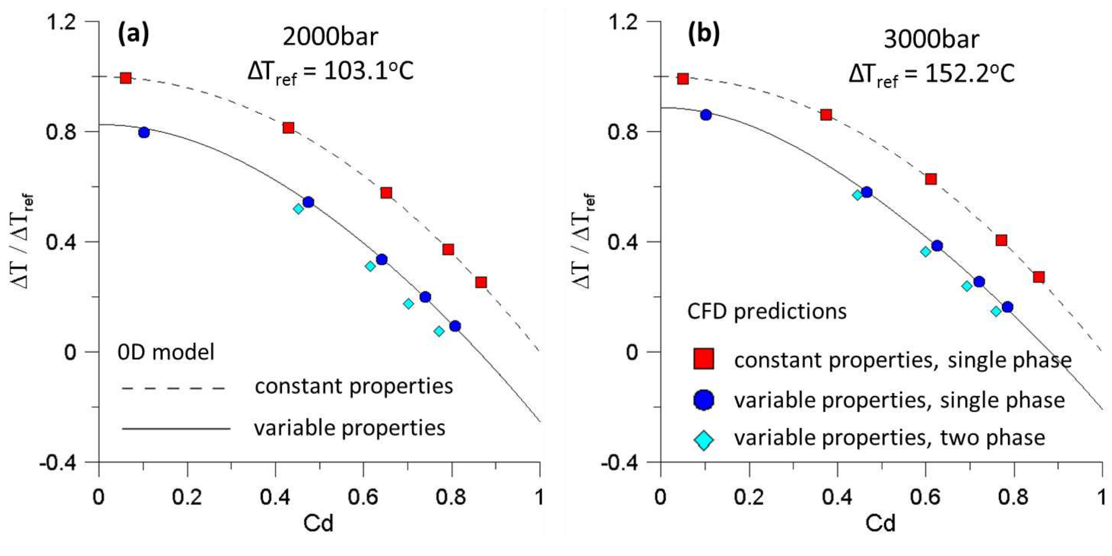

Fig.4: Dimensionless fuel heating for 2000bar (a) and 3000bar (b) inlet pressures. The effect of constant or variable properties assumption, as also the effect of two-phase flow is presented.

3.3 Moving lift simulations

In this section focus is given to the moving needle simulations which resemble a realistic fuel injection event. In these cases the needle lift law plays an important role, since an injection event has short duration and furthermore the closing phase is usually much shorter than the opening phase. This results in different fuel heating levels during the opening and closing phases of needle motion. In Fig.5a the needle lift law versus time is presented along with the fuel heating for the case of adiabatic nozzle wall with uniform initial fuel temperature distribution; two inlet pressures (2000 and 3000bar) are investigated for single and two phase flows. A strong fuel heating is observed at the initial opening of the needle, which is almost 70% higher for the higher inlet pressure of 3000bars (but approximately the same in dimensionless quantities in the order of 0.70-0.75ΔT_{ref}); the presence of the vapor phase does not seem to have any noticeable effect on the degree of fuel heating. The mean fuel exit heating reaches its maximum value at approximately 20μm needle lift. For the same needle lift, different fuel mass flow quantities are injected from the nozzle in the opening and the closing phases. This is due to the needle motion and the presence of the sac volume in which fuel mass is accumulated in the opening phase; in the closing phase the downward motion of the needle pushes the accumulated fuel mass from the sac volume to the nozzle’s exit and thus higher discharge coefficient is calculated. Integrating the instantaneous flow rate reveals that the total mass of the fuel injected during the injection event examined, is 8.33 and 10.05mg/hole for 2000bar and 3000bar inlet pressure respectively, while a 2% reduction in the overall mass injected was observed for the case of two-phase flow at 2000bar inlet pressure.

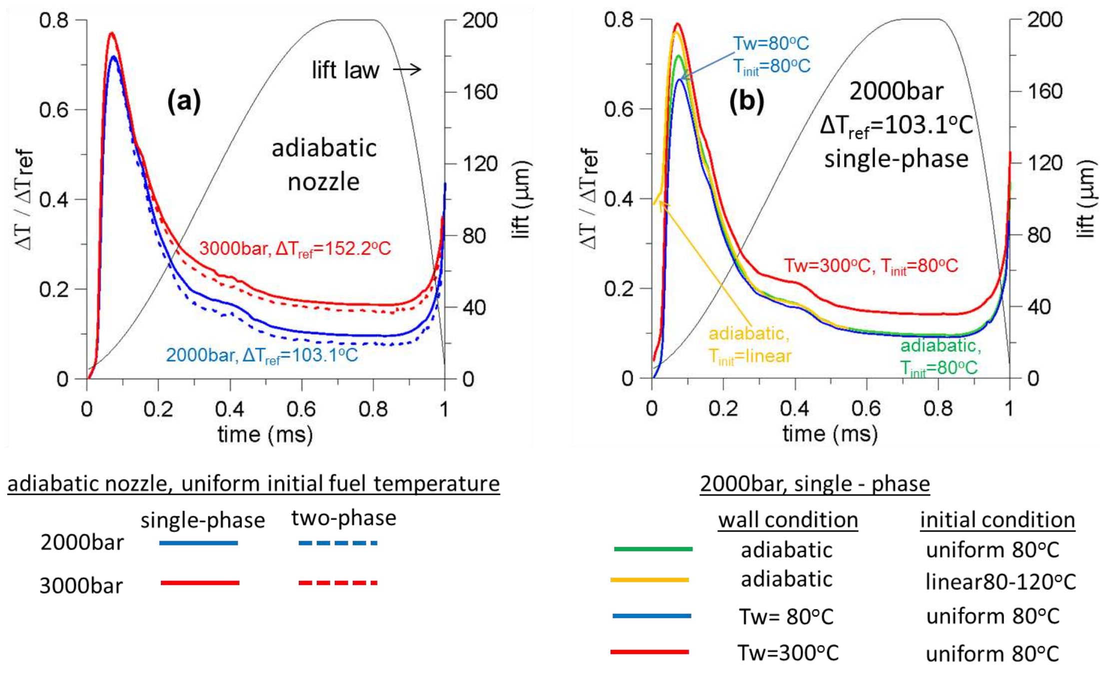

Fig.5:(a) Lift law and fuel heating versus time; solid lines refer to single-phase flow and dashed lines refer to two-phase flow. (b) Effect of initial and boundary conditions for fuel heating.

The effect of initial and boundary conditions is presented in Fig.5b for the case of 2000bar inlet pressure and single-phase flow. The case with uniform initial fuel temperature distribution and constant wall temperature equal to 300°C seems to enhance the fuel heating, but on the other hand this results to 0.25% overall mass flow reduction, which can be considered negligible. The case with constant wall temperature equal to the incoming fuel temperature (80°C) has a minor effect to the fuel heating compared to the adiabatic wall case; differences in maximum heating of $0.07\Delta T_{ref}$ compared to the adiabatic wall case are observed only at the initial stages of the opening phase. The case of adiabatic nozzle wall with a more realistic initial temperature distribution for the fuel is also presented in Fig.5b. The lower part of the fuel in the injector has initially a temperature of 120°C (equal to the fuel temperature at the end of the injection presented in Fig.5a), while the upper part of the fuel has the inlet temperature; between these two regions, a linear temperature distribution for the fuel was assumed. The curve corresponds to this case starts from a non-zero value, exhibits slightly higher maximum temperature, but the effect of initial condition is completely eliminated when the lift exceeds the 80μm. So, the effect of initial temperature distribution is of minor importance under the assumptions made. On the other hand, a more realistic approach would apply a conjugate heat transfer solution between the flow and the injector solid material with increased inlet fuel temperature; such an approach would require excessive computer resources and it was beyond the scope of the paper.

3.4 Flow field regimes

In this section the 3-D flow details are presented. In Fig.6 velocity streamlines colored with the velocity magnitude for the case of two-phase flow with 2000bar inlet pressure are presented along with sample cavitation bubbles; the velocity magnitude has been made non-dimensional with the reference velocity (661.3m/s for the case of 2000bar inlet pressure) and similar patterns are observed for the cases with 3000bar inlet pressure. Large vortical structures are observed in the sac volume with a low velocity magnitude. Inside the injector hole, the flow accelerates substantially reaching velocities of the order of 600m/s when the full lift is considered; the present model accounts for compressibility effects (in subsonic flows) as described in (Theodorakakos et al., 2014). At the inlet of the hole the flow turns direction and aligns with the axis of the hole. As a result, the pressure drops below the saturation pressure and bubbles are formed; under the influence of the velocity field, these are carried towards the nozzle exit, while bubble collapse and coalescence also take place. For this particular nozzle design examined, the needle motion does not seem to induce the Coanda effect (Trancossi, 2011) and the flow is directed from the passage to the inlet of the hole. This is attributed to the smooth needle profile, to the prolonged shape of the sac, as also to the elevated position of the hole relative to the sac volume.

Turning now our interest into the temperature field, the case of the full needle opening of 200μm is initially examined since during an injection event the needle lift remains most of the time at the full lift; furthermore no differences were identified between the steady state simulations and the transient simulations for this needle lift case. The effect of two-phase flow in the temperature predictions is presented in Fig.7a,b. In this figure the dimensionless temperature difference between the case of single-phase flow and two-phase flow is presented. As seen, the difference between these two fields is small (but locally may reach values in the order of $0.25\Delta T_{ref}$) and does not alter the overall heating of the fuel as it was shown in Fig.5a.

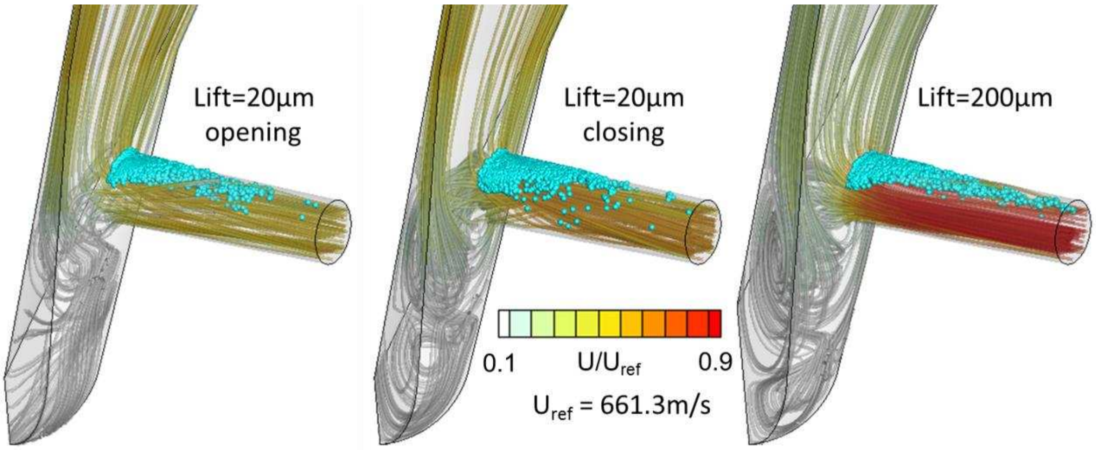

Fig.6: Dimensionless velocity field along with indicative cavitation bubbles for the case of two phase flow with 2000bar inlet pressure at 20μm lift (opening and closing phase) and 200μm.

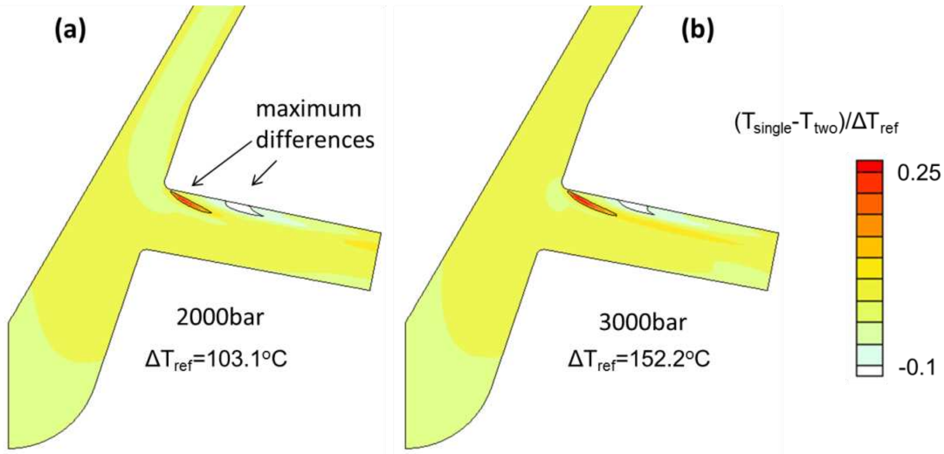

Fig.7: Dimensionless temperature difference between the single-phase and two-phase fields for the case of 200μm lift. (a) 2000bar inlet pressure, (b) 3000bar inlet pressure.

The effect of assuming constant or variable thermodynamic properties is presented in Fig.8 for the cases of single-phase flow with either constant or variable properties with 2000bar inlet pressure as also the case of single-phase flow with variable properties at 3000bar at 200μm needle lift. The maximum temperature is observed in the upper part of the inlet of the hole. In this region there are strong velocity gradients which induce friction and thus kinetic heating; for the case of variable properties the maximum dimensionless local temperature is approximately equal to ΔT_{ref} irrespective of the inlet pressure, while for the constant properties case the maximum dimensionless temperature is $1.26\Delta T_{ref}$. The variable properties case generally exhibits lower heating up values and additionally a sub-cooled liquid core is observed even inside the injector nozzle which vanishes near the nozzle exit; this behavior is not observed in the case with 3000bar inlet pressure.

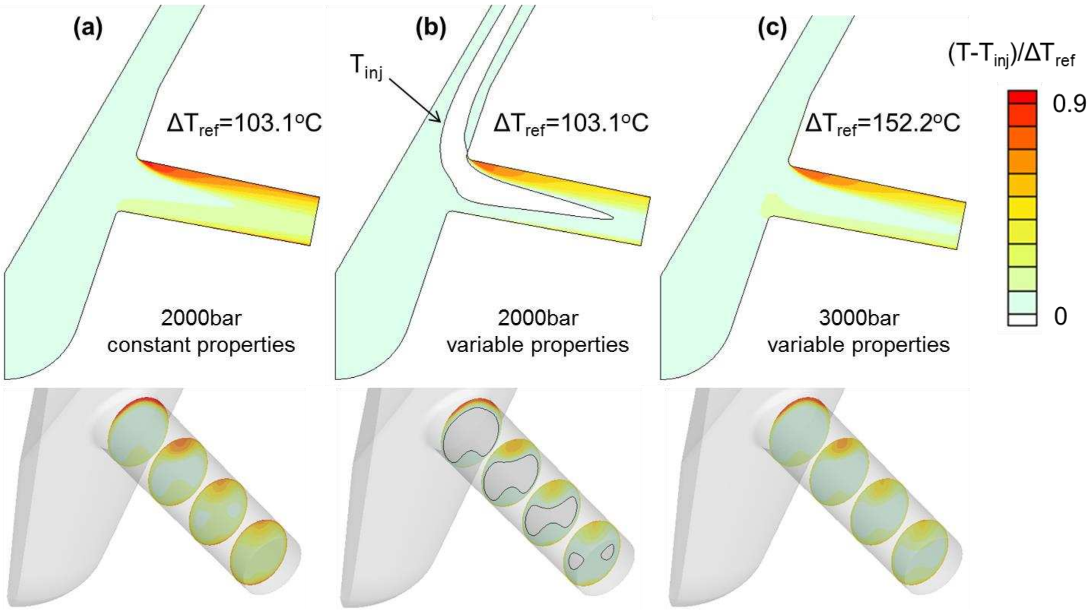

Fig.8: Dimensionless temperature field for the case of single phase flow at 200μm lift. (a) constant properties, 2000bar, (b) variable properties, 2000bar, (c) variable properties, 3000bar.

The transient effects in fuel heating for the case of single phase with 2000bar inlet pressure are presented in Fig.9 in which a comparison between the predictions for the opening and closing phase is performed; steady state predictions are also presented. Contrary to the case of full lift, in all other needle lift positions the temperature field exhibits a different behavior in opening and closing phase, since the needle motion affects the velocity field due to fuel incompressibility which in turn affects the temperature field, while the temperature "history" plays also an important role. The differences between the opening and the closing phase become more intense when the lift is low; these differences tend to vanish near the full lift. Initially the fuel in the whole computational domain has a uniform temperature (equal to zero in non-dimensional units). As the needle opens, the fuel is heated as it flows in the passage (not shown in Fig.9) and tends to fill the sac volume. Progressively as the lift increases the fuel is heated to a lower degree and the sac volume is filled with a cooler liquid having the temperature of the inlet. In the closing phase the downward needle motion pushes the "cold" fuel from the sac volume towards the hole. This transfer of mass from the sac to the hole, along with the higher velocities observed due to the needle motion lead to the development of a thinner thermal boundary layer in the closing phase. Near the inlet of the hole, a sub-cooled region exists at 80μm needle lift due to fuel depressurization, while this region is more evident in the closing phase.In the absence of Coanda effect, the maximum fuel temperature is always observed at the upper part of the inlet of hole, reaching values in the order of ΔT_{ref}.

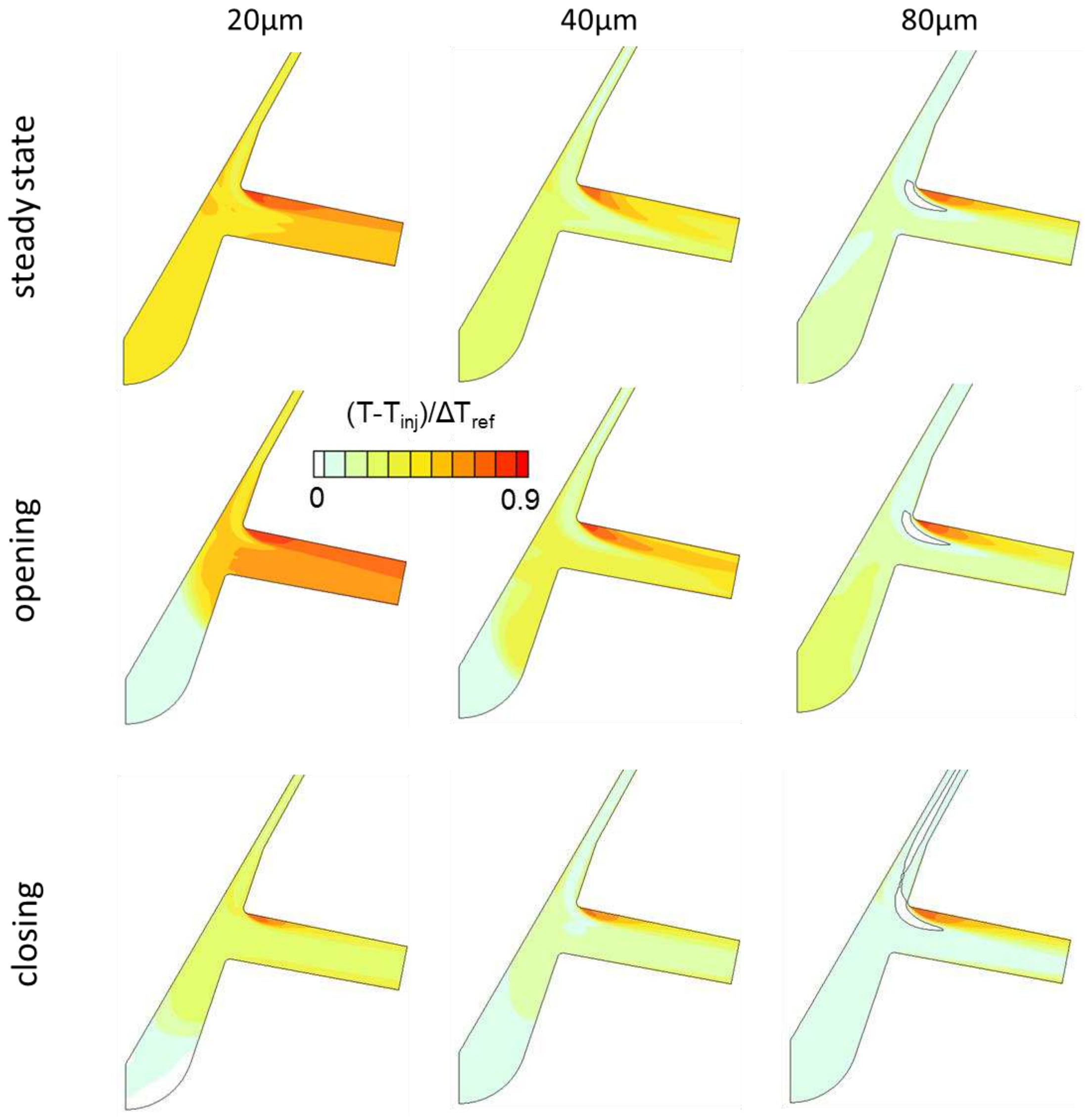

Fig.9: Temporal evolution of the dimensionless temperature field for the adiabatic nozzle. Comparison between the opening and the closing phases. Corresponding predictions from steady state simulations are also presented. 2000bar, single-phase, variable properties.

It is also of interest to examine the temperature field for the case of constant surface temperature equal to 300°C. This is presented in Fig.10 for the case of 2000bar inlet pressure with variable properties. As seen there is a thermal boundary layer developing near the wall which affects the temperature distribution, mainly in the sac area, when compared with the corresponding temperature field presented in Fig.9 for the case of adiabatic wall.

Furthermore, the sub-cooled region is suppressed for the constant temperature case, while it is evident that the needle motion affects the temperature field especially at low lifts. Regarding the case with constant surface temperature equal to 80ºC, the temporal evolution of dimensionless temperature in the opening phase is presented in Fig.11. This case evolves with the same fashion as the case with adiabatic nozzle wall and differences are observed only at the initial stages of the opening phase.

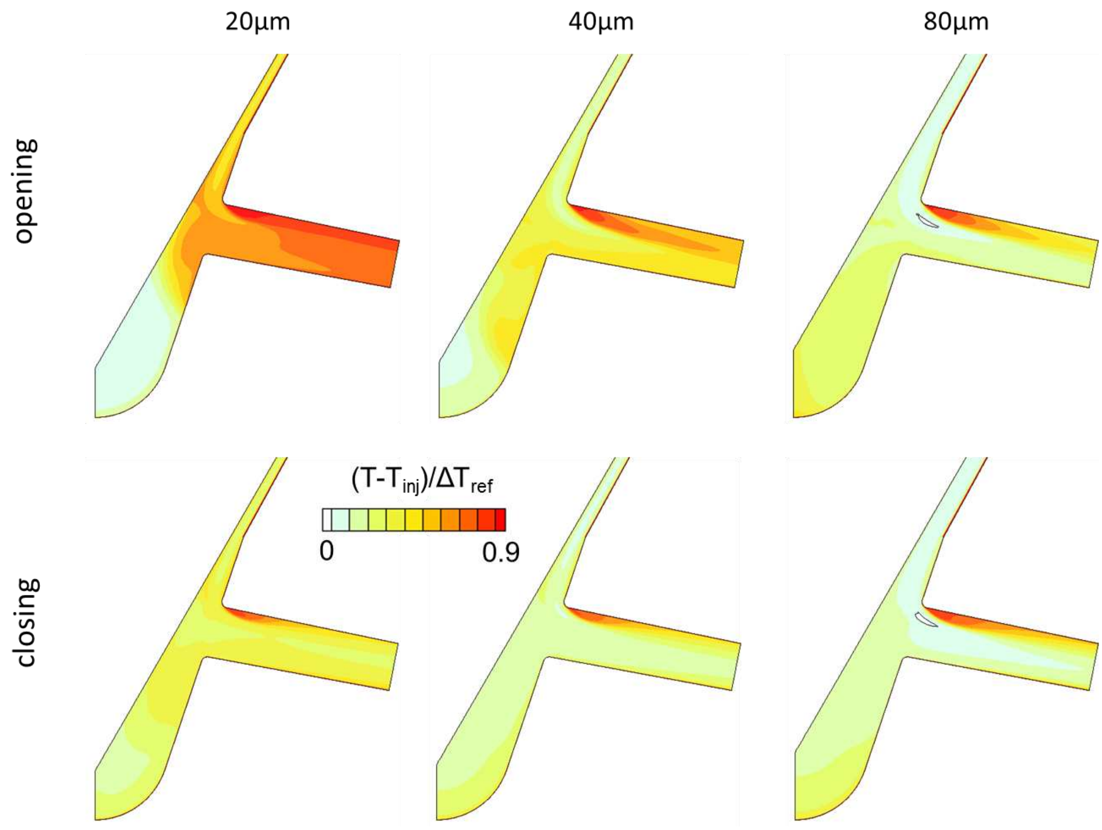

Fig.10: Temporal evolution of the dimensionless temperature field for the nozzle with constant surface temperature (300ºC). Comparison between the opening and the closing phases for the case of 2000bar inlet pressure.

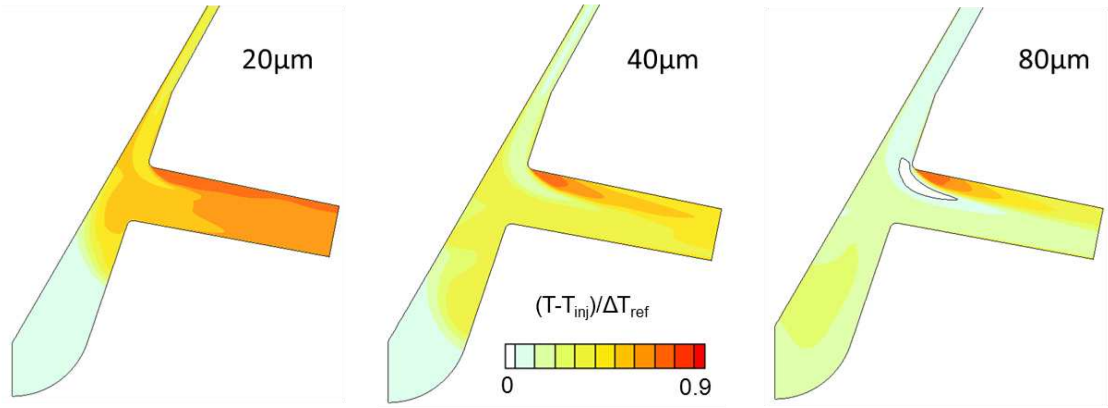

Fig.11: Temporal evolution of the dimensionless temperature field for the nozzle with constant surface temperature (80ºC, opening phase).

Under the assumption of adiabatic nozzle wall adopted here, the surface of the nozzle may reach high enough temperatures to induce the onset of heterogeneous boiling. Despite the fact that the present methodology does not account for such phenomena, an estimation of the boiling region can be performed by calculating the fuel boiling point according to the local pressure field and subtract it from the local temperature field. Since Diesel fuel consists of several components, a light (n-octane C_8H_{18}) and a heavy (n-hexadecane $C_{16}H_{34}$) have been chosen to estimate the boiling regions of these two components. In Fig.12a the nozzle surface temperature field for the case of two-phase flow with 2000bar and 3000bar inlet pressure at 200μm is presented. In Fig.12b the enlarged images represent the heterogeneous boiling regions for two Diesel species at the two corresponding inlet pressures. As seen, there is a region with a superheat degree ranging from 80 to 240K depending on the component type and inlet pressure. It is worth mentioning that this region on the nozzle's wall surface is quite close to the region inside the fluid volume in which cavitation occurs and bubbles are created but it is not identical.

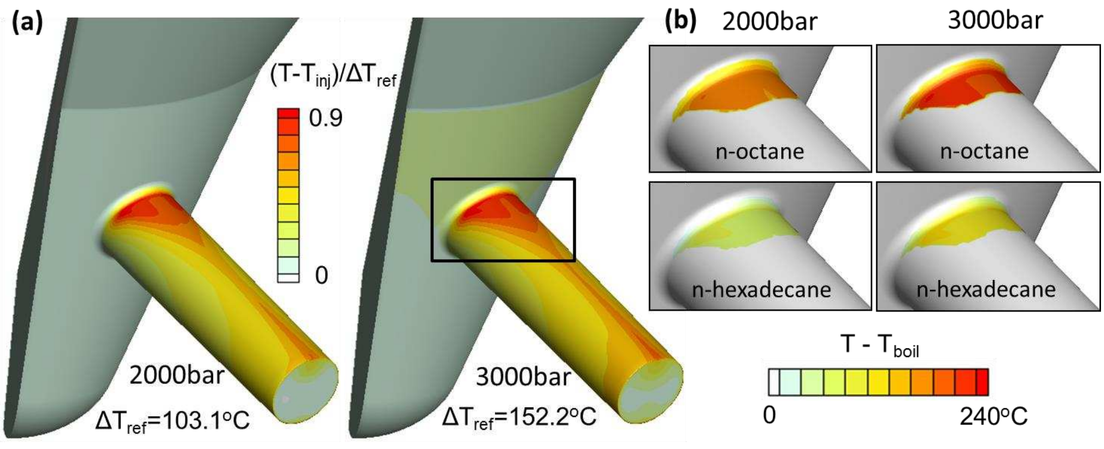

Fig.12:(a) Dimensionless surface temperature, (b) boiling overheat for a light and a heavy Diesel component. Two phase flow at 200μm liftfor the cases of 2000 and 3000bar inlet pressure.

4 Conclusions

A CFD model accounting for cavitation and thermal effects has been employed for investigating the flow and temperature field in high pressure Diesel injector nozzles. Cavitation is considered through a coupled Eulerian-Lagrangian formulation in which the temperature field is obtained via the solution of the total enthalpy equation accounting for the viscous heating effects. The thermal model has been initially validated against a 0-D thermodynamic model for an adiabatic nozzle showing a good performance for a wide range of steady lift positions. The effect of using constant or variable properties has been quantified revealing that the constant properties assumption may lead to large deviations in discharge coefficient and fuel heating predictions, especially in high pressure conditions in which fuel depressurization may lead to fuel sub-cooling. Transient simulations for moving lift cases have shown that the needle motion and the temperature history have a serious impact in predictions and steady lift simulations cannot represent the actual phenomenon, especially at low lifts. Temperature field exhibits differences in opening and closing phase which progressively diminish as the lift increases. The effect of cavitation is to reduce the flow rate due to blockage of the flow by the bubbles and reduce the fuel heating due to friction reduction. Finally, possible heterogeneous boiling regions have been identified for typical Diesel components, showing that the boiling region is very close to the cavitation region.

5 Acknowledgements

1. The research leading to these results has received funding from the People Programme (Marie Curie Actions) of the European Union's Seventh Framework Programme FP7/2007-2013/ under REA grant agreement n. 324313.
2. The scientific developments on the numerical solution of the RANS equations and the modeling of turbulence, scientific advances to which the honored scientists in the present volume, Professors B. E. Launder and K. Hanjalic have substantially contributed, made possible the reliable engineering solution of complex flows and the CFD as an industrial design tool.

6 Nomenclature

Romansymbols

Symbol	Description	Units
A	area	m^2
C_d	Discharge coefficient	-
c_p	Heat capacity	J/kgK
c_{pmT}	Mean heat capacity	J/kgK
D	diameter	μm
g	Gravity acceleration	m/s^2
h	enthalpy	J/kg
$\mathbf{I}$	Unit tensor	-
k	Turbulent kinetic energy	m^2/s^2
p	pressure	Pa
Pr	Prandtl number	-
S_h	Source term	W/m^3
T	temperature	K
t	time	s
U, $\mathbf{u}$	velocity	m/s

Greeksymbols

Symbol	Description	Units
a	Volume fraction	-
κ	Thermal conductivity	W/mK
μ	viscosity	kg/ms
ρ	density	kg/m^3
$\boldsymbol{\tau}$	Stress tensor	N/m^2

Subscripts

Symbol	Description
0	At reference point
add	additional

eff	effective
in	inlet
init	initial
inj	injection
L	liquid
lam	Laminar
m	mean
out	outlet
single	Single phase
tot	total
turb	turbulent
two	Two phase
w	wall

References

Alajbegovic, A., Grogger, H.A., Philipp, H., 1999. Calculation of Transient Cavitation in Nozzle Using the Two-Fluid Model, Proc. 12th ILASS, Indianapolis, Indiana, USA.

Ando, K., Colonius, T., Brennen, C., 2011. Numerical simulation of shock propagation in a polydisperse bubbly liquid. International Journal of Multiphase Flow 37, 596–608.

Andriotis, A., Gavaises, M., C., A., 2008. Vortex flow and cavitation in diesel injector nozzles. Journal of Fluid Mechanics 610, 195–215.

Arcoumanis, C., Badami, M., Flora, H., Gavaises, M., 2000. Cavitation in Real-Size Multi-Hole Diesel Injector Nozzles. SAE Paper 2000-01-1249.

Badock, C., Wirth, R., Fath, A., Leipertz, A., 1999. Investigation of cavitation in real size diesel injection nozzles. International Journal of Heat and Fluid Flow 20, 538-544.

Battistoni, M., Grimaldi, C.N., 2012. Numerical analysis of injector flow and spray characteristics from diesel injectors using fossil and biodiesel fuels. Applied Energy 97, 656-666.

Blessing, M., König, G., Krüger, C., Michels, U., Schwarz, V., 2003. Analysis of Flow and Cavitation Phenomena in Diesel Injection Nozzles and its Effect on Spray and Mixture Formation. SAE Paper 2003-01-1358.

Brennen, C.E., 1995. Cavitation and Bubble Dynamics. Oxford University Press, New York; Oxford.

Chaves, H., Knapp, M., Kubitzek, A., Obermeier, F., 1995. Experimental Study of Cavitation in the Nozzle Hole of Diesel Injectors Using Transparent Nozzles. SAE Paper 950290.

Chen, Y.L., Heister, S.D., 1995. Two-Phase Modeling of Cavitated Flows. Computers & Fluids 24, 799-809.

ExxonMobil, The outlook for energy: A view to 2040.

Fuster, D., Colonius, T., 2011. Modelling bubble clusters in compressible liquids. Journal of Fluid Mechanics 1, 1–38.

Giannadakis, E., Gavaises, M., Arcoumanis, C., 2008. Modelling of cavitation in diesel injector nozzles. Journal of Fluid Mechanics 616, 153–193.

Giannadakis, E., Gavaises, M., Roth, H., Arcoumanis, C., 2004. Cavitation Modelling in Single-Hole Diesel Injector Based on Eulerian-Lagrangian Approach, Proc. THIESEL International Conference on Thermo- and Fluid Dynamic Processes in Diesel Engines, Valencia, Spain.

Giannadakis, E., Papoulias, D., Gavaises, M., Arcoumanis, C., Soteriou, C., Tang, W., 2007. Evaluation of the predictive capability of diesel nozzle cavitation models. SAE Technical Paper 2007-01-0245.

Goud M, Greif D, Suffa M, Winklhofer E, Gill D, 2012. Virtual erosion prediction, design optimisation and combustion system integration of high pressure fuel injector systems. IMechE Conf Fuel Injection Systems for IC Engines, London.

Habchi, C., Dumont, N., Simonin, O., 2008. Multidimentional simulation of cavitating flows in diesel injectors by a homogeneous mixture modeling approach. Atom. Sprays 18, 129-162.

He, Z., Zhong, W., Wang, Q., Jiang, Z., Fu, Y., 2013. An investigation of transient nature of the cavitating flow in injector nozzles. Applied Thermal Engineering 54, 56-64.

Hilgenfeldt, S., Brenner, M.P., Grossmann, S., Lohse, D., 1998. Analysis of rayleigh-plesset dynamics for sonoluminescing bubbles. Journal of Fluid Mechanics 365, 171–204.

Jamaluddin, A., Ball, G., Turangan, C., Leighton, T., 2011. The collapse of single bubbles and approximation of the far-field acoustic emissions for cavitation induced by shock wave lithotripsy. Journal of Fluid Mechanics 677, 305–341.

Javier López, J., Salvador, F.J., de la Garza, O.A., Arrègle, J., 2012. A comprehensive study on the effect of cavitation on injection velocity in diesel nozzles. Energy Conversion and Management 64, 415-423.

Keller, J., Miksis, M., 1980. Bubble oscillations of large amplitude. Journal of the Acoustical Society of America 68, 628–633.

Kolev, N., 2002. Multiphase Flow Dynamics 3: Turbulence, Gas Absorption and Release, Diesel Fuel Properties. Springer.

Launder, B.E., Spalding, D.B., 1974. The numerical computation of turbulent flows. Computer Methods in Applied Mechanics and Engineering 3, 269-289.

Lee, W.G., Reitz, R.D., 2010. A Numerical Investigation of Transient Flow and Cavitation Within Minisac and Valve-Covered Orifice Diesel Injector Nozzles. J. Eng. Gas Turbines Power 132.

Liu, T.G., Khoo, B.C., Xie, W.F., 2004. Isentropic one-fluid modelling of unsteady cavitating flow. Journal of Computational Physics 201, 80-108.

Margot, X., Hoyas, S., Fajardo, P., Patouna, S., 2010. A moving mesh generation strategy for solving an injector internal flow problem. Mathematical and Computer Modelling 52, 1143-1150.

Neroorkar, K.D., Mitcham, C.E., Plasas, A.H., Grover, R.O., Schmidt, D.P., 2012. Simulations and Analysis of Fuel Flow in an Injector Including Transient Needle Effects, ILASS-Americas, San Antonio.

Payri, F., Bermúdez, V., Payri, R., Salvador, F.J., 2004. The influence of cavitation on the internal flow and the spray characteristics in diesel injection nozzles. Fuel 83, 419-431.

Payri, F., Margot, X., Patouna, S., Ravet, F., Funk, M., 2009. A CFD Study of the Effect of the Needle Movement on the Cavitation Pattern of Diesel Injectors. SAE Technical Paper 2009-24-0025.

Payri, F., Payri, R., Salvador, F.J., Martínez-López, J., 2012. A contribution to the understanding of cavitation effects in Diesel injector nozzles through a combined experimental and computational investigation. Computers & Fluids 58, 88-101.

Payri, R., Salvador, F.J., Gimeno, J., Venegas, O., 2013. Study of cavitation phenomenon using different fuels in a transparent nozzle by hydraulic characterization and visualization. Experimental Thermal and Fluid Science 44, 235-244.

Prosperetti, A., Hao, Y., 1999. Modelling of spherical gas bubble oscillations and sonoluminescence. Philosophical Transactions of the Royal Society of London Series A-Mathematical Physical and Engineering Sciences 357, 203-223.

Salvador, F.J., Martínez-López, J., Romero, J.V., Roselló, M.D., 2013. Computational study of the cavitation phenomenon and its interaction with the turbulence developed in diesel injector nozzles by Large Eddy Simulation (LES). Mathematical and Computer Modelling 57, 1656-1662.

Singhal, A.K., Athavale, M.M., Li, H.Y., Jiang, Y., 2002. Mathematical basis and validation of the full cavitation model. Journal of Fluids Engineering-Transactions of the ASME 124, 617-624.

Soteriou, C., Andrews, R., Smith, M., Torres, N., Sankhalpara, S., 2000. The flow patterns and sprays of variable orifice nozzle geometries for diesel injection. SAE Paper 2000-01-0943.

Städtke, 2007. Gasdynamic Aspects of Two-Phase Flow. Wiley-VCH Verlag GmbH and Co. KGaA.

Strotos, G., Koukouvinis, P., Theodorakakos, A., Gavaises, M., 2014a. Quantification of Friction-induced Heating in tapered Diesel orifices, SIA POWERTRAIN, Rouen, France.

Strotos, G., Koukouvinis, P., Theodorakakos, A., Gavaises, M., Wang, L., Li, J., McDavid, R.M., 2014b. Fuel heating in high pressure diesel nozzles, THIESEL, Valencia, Spain.

Theodorakakos, A., Mitroglou, N., Strotos, G., Atkin, C., Gavaises, M., 2014. Friction-induced heating in nozzle hole micro-channels under extreme fuel pressurisation. FUEL 123, 143-150.

Trancossi, M., 2011. An Overview of Scientific and Technical Literature on Coanda Effect Applied to Nozzles. SAE Technical Paper 2011-01-2591.

Versteeg, H.K., Malalasekera, W., 2007. An Introduction to Computational Fluid Dynamics: The finite volume method (2nd Edition).

Wolfshtein, M., 1969. The velocity and temperature distribution in one-dimensional flow with turbulence augmentation and pressure gradient. International Journal of Heat and Mass Transfer 12, 301-318.

Yuan, W., Schnerr, G.n.H., 2004. Numerical Simulation of Two-Phase Flow in Injection Nozzles: Interaction of Cavitation and External Jet Formation. Journal of Fluids Engineering 125, 963-969.

Zeravcic, Z., Lohse, D., Saarloos, W., 2011. Collective oscillations in bubble clouds. Journal of Fluid Mechanics 680, 114–149.

Zhao, H., Quan, S., Dai, M., Pomraning, E., Senecal, P.K., Xue, Q., Battistoni, M., Som, S., 2013. Validation of a Three-Dimensional Internal Nozzle Flow Model Including Automatic Mesh Generation and Cavitation Effects, ASME 2013 Internal Combustion Engine Division Fall Technical Conference.